

Contents lists available at ScienceDirect

JCIS Open

journal homepage: www.journals.elsevier.com/jcis-open



On the rheology of linear wormlike micellar solutions

Krassimir D. Danov a,b,* O, Gergana M. Radulova b, Jordan T. Petkov b, Yee Wei Ung d

- a Department of Chemical & Pharmaceutical Engineering, Faculty of Chemistry & Pharmacy, Sofia University "St. Kliment Ohridski", 1164, Sofia, Bulgaria
- ^b Center of Competence "Smart Mechatronic, Eco- and Energy-saving Systems, and Technologies", Bulgaria
- ^c Biological Physics, School of Physics and Astronomy, The University of Manchester, Schuster Building, Oxford Road, M13 9PL, UK
- d KLK OLEO, KL-Kepong Oleomas Sdn Bhd, Menara KLK, Jalan PJU 7/6, Mutiara Damansara, 47810, Petaling Jaya, Selangor Dalur Ehsan, Malaysia

ARTICLE INFO

Keywords: Poisson renewal model Shuffling model Shear rheology Linear wormlike micellar solutions Elasticity Breaking and reptation times

ABSTRACT

The shear rheology of linear wormlike micellar solutions (WMSs) is described by both Poisson renewal (PRM) and shuffling (SFM) models with different values of the model parameters. For low shear strains and rates of strains, the micellar solutions behave as a Maxwellian body with constant elasticity and viscosity. The excellent description of experimental data in the literature using PRM or SFM suggests that both models predict identical dependencies of the dynamic storage and loss moduli on the frequency of oscillations. It is shown in the literature, that the PRM becomes equivalent to the SFM, when the breaking time is constant, $\tau_{\rm br}$, and the characteristic reptation time, $\tau_{\rm rep}$, is equal to $\pi^2 \tau_{\rm d0}$, where $\tau_{\rm d0}$ is the reptation time evaluated with respect to the average length of the chain. Three independent rheological tests (apparent viscosity vs shear rate, stress vs strain at constant shear rates, strain oscillations at low amplitudes and different frequencies) are applied to low, medium, and high zero-shear viscosity WMSs to obtain the PRM and SFM model parameters (elasticity, viscosity, relaxation, breaking, and reptation times). The known closed-form analytical expression for the Laplace image of the stress relaxation function and the respective infinite series for the complex modulus give possibility for the reported here precise systematic calculations of the storage and elastic moduli, the crossover frequency, and the elasticity for all values of $\zeta_{br}= au_{br}/ au_{rep}\leq 100$. The predictions of the PRM length-dependent breaking-time versions are indistinguishable from those of the SFM for the obtained universal dependencies of the characteristic time, τ_{B0} , on ζ_{br} . The applicability of the Vasquez-Cook-McKinley and the single-mode Oldroyd 8-constant models to describe the rheological behavior of WMSs is tested. The theoretical findings and conclusions are confirmed experimentally and illustrate the self-consistency of the used rheological regimes.

1. Introduction

At higher concentrations, the molecules in solutions of surface-active substances (surfactants) self-assemble to form giant wormlike and branched micelles [1]. Under certain conditions, the branched micelles assemble into a multiconnected micellar network that represents a supergiant micelle [2–5]. Micelle growth is accompanied with a significant increase of the viscosity of the solutions. Such concentrated surfactant solutions find wide applications in the formulations for personal care and house-hold detergency [6,7]. Examples are the shampoos, body washes, cosmetic formulations, liquid laundry detergents, formulations for dishwashing and home cleaning, etc. Similar micellar systems are used also in drug delivery, oilfield industry, and turbulent drag-reduction [8,9]. The competition between the

companies-producers has led to the use of novel surfactant molecules and additives in order to improve the properties of the formulations with respect to their washing action, skin and eye irritation action, stability and durability, biodegradability, and tolerance to hard water.

The wormlike micelles growth is observed in a wide range of systems: in nonionic surfactant solutions at higher concentrations and temperature [10,11]; in ionic surfactant solutions in the presence of salts, zwitterionic and nonionic co-surfactants, etc. [1,12–16]; in gemini surfactants, lipids, and biological surfactant systems [1]; block copolymer can also self-assemble into giant wormlike micelles [17]. For practical applications, the wormlike micellar solutions (WMSs) are convenient because their rheological properties (viscosity and elasticity) can be adjusted over a wide range by tunning the salt, co-surfactant, perfumes, etc. concentrations [18,19]. In industrial applications, the

E-mail address: kd@lcpe.uni-sofia.bg (K.D. Danov).

^{*} Corresponding author. Department of Chemical & Pharmaceutical Engineering, Faculty of Chemistry & Pharmacy, Sofia University "St. Kliment Ohridski", 1164, Sofia, Bulgaria.

rheological characteristics of detergents, cosmetics, and pharmaceuticals are of crucial importance for the quality of the final products. At low shear strains and rates of strains, the rheological parameters of WMSs are usually compared with the predictions of the Maxwell model of viscoelastic body with constant shear elasticity $G_{\rm M}$, zero-shear viscosity η_0 , and relaxation time $\tau_{\rm R}=\eta_0/G_{\rm M}$. In the case of Maxwell model, the dynamic complex modulus, $G^*=G'+iG''$, defined with respect to the dynamic storage, G', and loss, G'', moduli and obtained from the oscillatory experiments with frequency ω and low shear strain amplitudes obeys the following equation:

$$\frac{G^{*}(\omega)}{G_{\rm M}} = \frac{i\omega\tau_{\rm R}}{1 + i\omega\tau_{\rm R}} \tag{1}$$

The basic properties of the storage and loss moduli are: $G'(\omega) \to G_{\rm M}$ and $G''(\omega) \to 0$ for large frequencies, $\omega \tau_{\rm R} \gg 1$; the $G'(\omega)$ and $G''(\omega)$ curves intersect in the crossover frequency, $\omega = 1/\tau_{\rm R}$, where $G'(1/\tau_{\rm R}) = G''(1/\tau_{\rm R}) = G_{\rm M}/2$; $G''(\omega)$ has a maximum at $\omega = 1/\tau_{\rm R}$; $G''(\omega)$ plotted against $G'(\omega)$ parametrically eliminating the frequency information is a perfect semicircle (Cole-Cole plot). Even at low shear strains, the rheological responses of WMSs can deviate (to different extent) from the pure Maxwellian behavior at high shear rates (large values of the frequency).

In the literature [20-26], the term "linear wormlike micellar solutions" is used to point out that the physical parameters of the respective rheological models (elasticity, viscosity, characteristic times, etc.) do not depend on the shear strain and on the rate of strain magnitudes. In the case of linear wormlike micelles, Cates and coauthors [20-26] developed statistical theory, which accounts for the curvilinear diffusion of linear molecules confined by their neighbors (reptation), the micelle reversible scission and end-interchange processes. The process of reptation is characterized by the reptation time, $\tau_{\rm rep}$, and the reaction of micelle reversible breakage and recombination is scaled with the mean breaking time, $\tau_{\rm br}$. The reptation-reaction model predicts that for small ratios, $\zeta_{br} = \tau_{br}/\tau_{rep}$, and not too high shear rates, the stress relaxation in the WMS is exponential with one relaxation time $\tau_{\rm R} \propto (\tau_{\rm br} \tau_{\rm rep})^{1/2}$. The practical application to experimental data across all frequencies was put forward by Granek and Cates [27] in their landmark Poisson renewal model (PRM). An inspection of the assumptions and approximations of the PRM suggests that the length-independent renewal time connects with a better physical interpretation of the true reversible scission process [28,29]. This reinterpretation of the PRM has been called the shuffling model (SFM). The extensions of PRM and SFM, including additional stress relaxation processes, are reported in the literature for contour length fluctuations, intra-tube Rose modes (flexible and semi-flexible), double reptation [27-31]. The rheological models for branched wormlike micelles are considered in Refs. [32-35].

In the literature [29], it is pointed out that: i) the PRM did not admit a closed-form solution; ii) the SFM gives a simple expression for the dynamic complex modulus, G^* ; iii) the expression given for the reptation time, τ_{rep} , drops the coefficient of π^2 , as it was done in the original PRM and SFM, but the pointer model [30,31] includes it. In many cases, the experimentalists obtain different values for $\tau_{\rm br}$ and $\tau_{\rm rep}$ processing given experimental data for $G^*(\omega)$ using these models. This problem appears because of typos in some publications related to the PRM and SFM. For example, the typos in Eq. (15) from Ref. [29] written for the PRM lead to the wrong predicted values for the shear modulus, G_e , and the reptation time, τ_{rep} . Here, we focus on the data processing of independent rheological measurements with an emphasis on the interpretation of the obtained rheological data on the basis of rheological models. In Section 2, the ingredients in the investigated WMSs and the used experimental methods are briefly described. Section 3 is dedicated to represent the available results for the closed-form solution of the PRM for constant breaking times, the exact infinite series for calculation of the complex modulus, G^* , and the relationships between parameters

used in PRM and SFM. These theoretical results are applied for precise calculations of both moduli, dimensionless crossover frequencies, ratios between the crossover dynamic modulus and the shear modulus, etc. for all values of $\tau_{\rm br}/\tau_{\rm rep}. \leq 100.$ In Section 4, the experimental data obtained from three rheological tests applied to different wormlike micellar solutions are processed and the self-consistency of the obtained results is discussed. The applicability of the general form of the PRM, the Vasquez–Cook–McKinley model [37–39], and the single-mode Oldroyd 8-constant model [40], are discussed in Section 5. The main conclusions are summarized in Section 6. For the clarity of the main text, some experimental data are included and the main theoretical expressions corresponding to PRM and SFM are re-derived in the Supplementary material.

The paper could be useful for a broad audience of researchers, who use rheological data to characterize and compare the wormlike micellar solutions, and it shows the interrelationships between the studied rheological models.

2. Materials and methods

For the rheological experiments, we used mixed WMSs composed of different ionic and zwitterionic surfactants: i) anionic surfactants sodium dodecyl sulfate (SDS), product of Sigma-Aldrich, active substance 100 %, and palmitic sulfonated methyl ester (C_{16} SME), product of KLK OLEO, purity of 96 %; ii) zwitterionic surfactants cocamidopropyl betaine (CAPB), product of Evonik, Essen, Germany, Tego Betain F 50, active substance 37.8 %, and N,N-dimethyldodecylamine N-oxide (DDAO), product of Sigma-Aldrich, active substance 30 %. These samples were used in our experiments without any additional purification.

The aqueous solutions were prepared with deionized water purified by Elix 3 water purification system (Millipore). All experiments were carried out at a temperature of 25 °C. The studied 12 wt% mixed SDS + CAPB and SDS + DDAO solutions of weight ratio 3:7 and 15 wt% C_{16} SME + CAPB of weight ratio 1:3 contain linear wormlike micelles [19,41].

Rotational rheometer Discovery Hybrid Rheometer HR20 (TA Instruments, Delaware, USA) equipped with cone-plate geometry CP 2/40 was used to measure the rheological response of the micellar solutions. The temperature, $T=25\pm0.1$ °C, was controlled by a Peltier element. The evaporation was suppressed by a solvent trap. To confirm the reproducibility of the data, each rheological experiment was repeated at least three times starting with newly prepared solutions. Three different rheological regimes were applied to characterize the shear rheology of the studied solutions. First, we measured the apparent viscosity, $\eta_{\rm app}$ (the ratio between the steady shear stress and the rate of shear strain). The steady shear rate sweeps were performed in the shear rate range from 0.001 to $1000~\text{s}^{-1}$, using a logarithmic profile with approximately 25 data points per decade. The rheometer automatically adjusted the acquisition time at each point to ensure steady-state conditions, based on a torque stability criterion of 1 % deviation. The storage and loss moduli, G' and G'', as functions of the angular frequency, ω , in the range from 0.06 to 300 rad/s at a small amplitude of the shear strain (0.02) were obtained using the frequency sweep oscillatory regime. We checked the linear rheological response of all micellar solutions - the obtained moduli were independent on the amplitude of the shear strain up to 0.1 over the studied frequency range.

To obtain the parameters of the Maxwell model (shear elasticity $G_{\rm M}$ and viscosity η_0), we measured the shear stress, $\sigma(t)$, and the shear strain, $\gamma(t)$, as functions of time, t, for all solutions at low constant shear rates, $d\gamma/dt$. Fig. 1 shows the respective dependencies in the case of 15 wt% (1:3) $C_{16}SME + CAPB$ micellar solution. The used rheometer produces a well-defined linear dependence of the shear strain on time with a rate of shear strain of 0.0979 ± 0.0001 s⁻¹ and a regression coefficient of 0.9999 (Fig. 1). In the case of a constant shear rate, $d\gamma/dt$, the Maxwell

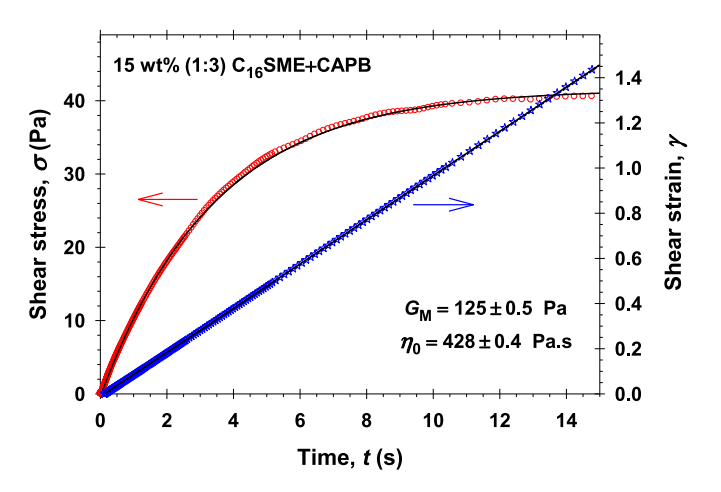


Fig. 1. Dependence of shear strain $\gamma(t)$ and shear stress $\sigma(t)$ on time t, measured for 15 wt% (1:3) C₁₆SME + CAPB micellar solution.

model predicts the following simple exponential dependence of the shear stress on time:

$$\sigma(t) = \eta_0 \frac{\mathrm{d}\gamma}{\mathrm{d}t} \left[1 - \exp\left(-\frac{G_{\mathrm{M}}}{\eta_0}t\right) \right] \tag{2}$$

The solid line in Fig. 1 represents the best fit of $\sigma(t)$ according to Eq. (2). The obtained best fit parameters from this particular run are $G_{\rm M}=125\pm0.5$ Pa and $\eta_0=428\pm0.4$ Pa s with regression coefficient of 0.9998.

More details regarding the data processing of all experimental data obtained with the use of the different rheological regimes are discussed in Sections 4 and 5.

3. Closed-form solution of the PRM and interrelationships between PRM and SFM

In the original PRM, the stress relaxation function, G(z,t), of polymer solution with shear modulus $G_{\rm e}$, corresponding to a chain of length L scaled with the average chain length, $L_{\rm a}$, is described by a multi-exponential decay of time t [42]:

$$\frac{G(z,t)}{G_{\rm e}} = \frac{8}{\pi^2} \sum_{p={\rm odd}}^{\infty} \frac{1}{p^2} \exp\left[-\frac{p^2 t}{\tau_{\rm d}(z)}\right] \text{ and } z \equiv \frac{L}{L_{\rm a}}$$
 (3)

Here the reptation time of the *L*-chain, $\tau_{\rm d}(z)$, is related to the dimensionless chain length, z, and the reptation time, $\tau_{\rm d0}$, evaluated with respect to the average length of the chain, $L_{\rm a}$, as follows: $\tau_{\rm d}=\tau_{\rm d0}z^3$. The Laplace transform with respect to time t defines the relaxation of the irreversible system in the Laplace space:

$$G_{\rm L}(z,s) \equiv \int_{0}^{\infty} \frac{G(z,t)}{G_{\rm e}} \exp(-st) dt = \frac{8}{\pi^2} \sum_{p={\rm odd}}^{\infty} \frac{\tau_{\rm d}}{p^2(p^2 + \tau_{\rm d}s)}$$
(4)

In the Supplementary material (S1), we alternatively prove the following exact closed-form expression for the series in the right-hand side of Eq. (4):

$$G_{\rm L}(z,s) = \frac{1}{s} - \frac{1}{s} \frac{\tanh(u)}{u} \text{ and } u \equiv \frac{z^{3/2}}{2} (\pi^2 \tau_{\rm d0} s)^{1/2}$$
 (5)

The waiting time distribution for a renewal event to occur on a chain of length L is scaled by characteristic time $\tau_B(L)$. Different concrete dependencies of τ_B on $z=L/L_a$ are discussed in the literature [27,29]: a) in the case of reversible scission rearrangements, the following expression for the characteristic time is defined:

$$\tau_{\rm B}(z) = \frac{3.3\tau_{\rm B0}}{2+z} \tag{6a}$$

 b) if the linear wormlike micelles rearrange by the end attack pathway, one obtains:

$$\tau_{\rm B}(z) = \frac{4.0\tau_{\rm B0}}{1+z} \tag{6b}$$

Here τ_{B0} has a meaning of a characteristic breaking time. Finally, the dynamic complex modulus, G^* , is calculated by the averaging over the equilibrium micellar length distribution, see Eqs. (S9) and (S10), to derive the following relationship [27]:

$$\frac{G^{\star}(\omega)}{G_{\rm e}} = \frac{i\omega \langle G_{\rm L}(z, i\omega + \tau_{\rm B}^{-1}) \rangle}{1 - \langle \tau_{\rm B}^{-1} G_{\rm L}(z, i\omega + \tau_{\rm B}^{-1}) \rangle}$$
(7)

In the recent publication [29], the authors "argue that a constant $\tau_{\rm B}$ (rather that the L-dependent one used in the original PRM) will provide a better approximation of the essential Cates mechanism, because it gives the true rate at which slow-relaxing interior segments are "renewed", i. e., transformed to fast-relaxing end segments". Thus, the PRM should be compared with the SFM using the characteristic breaking time, $\tau_{\rm B}(z)=\tau_{\rm br}$. In this case, Eq. (7) is simplified and it yields:

$$\frac{G^*(\omega)}{G_o} = \frac{i\omega\tau_{\rm br}(1-F)}{i\omega\tau_{\rm br} + F} \tag{8}$$

Here the universal function, $F(\beta)$, depends only on one complex parameter, β , expressed through the frequency, ω , the reptation time, τ_{d0} , evaluated with respect to the average chain length, and the constant breaking time, τ_{br} . It is shown in the Supplementary material (S3), that the function, F, is given by the following series:

$$F(\beta) = \frac{2\pi^{1/2}}{\beta^{1/2}} + \sum_{m=0}^{\infty} \frac{b_m}{\beta^{(2+m)/3}} \text{ and } \beta \equiv \left(\frac{\pi^2 \tau_{d0}}{\tau_{br}}\right) (1 + i\omega \tau_{br})$$
(9)

The exact numerical values of the coefficients, b_0 , b_1 , ..., are calculated using Eq. (S19), see Ref. [36]. For convenience, we define function $F(\beta) = 1 - \beta C(\beta)$, where $C(\beta)$ is introduced in Ref. [36]. The series defined by Eq. (9) gives the possibility to calculate the values of the dynamic complex modulus with a relative precision of 10^{-14} using the double precision definitions in Fortran for all values of the complex parameter, β . It is obvious from the definition of β , Eq. (9), and the asymptotic expression given by Eq. (S20b) that the larger the values of the dimensionless frequency, $\omega \tau_{\rm br}$, and/or the ratio, $\tau_{\rm d0}/\tau_{\rm br}$, the faster the convergence of the series in Eq. (9) is. For large values of $\tau_{\rm br}/\tau_{\rm d0}$, the number of terms in the series needed to calculate $F(\beta)$ with a good precision considerably increases [36].

In the Supplementary material (S4), the main result from the SFM for the dynamic complex modulus, G^* , is briefly discussed. The final conclusion is that: if the breaking time, $\tau_{\rm B}(z)$, in the PRM is assumed to be a constant equal to the characteristic breaking time, $\tau_{\rm br}$, and the characteristic reptation time, $\tau_{\rm rep}$, is defined to be $\tau_{\rm rep} = \pi^2 \tau_{\rm d0}$, where $\tau_{\rm d0}$ is the reptation time evaluated with respect to the average chain length, $L_{\rm a}$, then both PRM and SFM predict the same dependencies of the dynamic modulus, G^* , on the frequency, ω , the characteristic reptation, $\tau_{\rm rep}$, and the mean breaking, $\tau_{\rm br}$, times. Moreover, for large values of $|\beta| \gg 1$ (small values of $\zeta_{\rm br} = \tau_{\rm br}/\tau_{\rm rep} \ll 1$) and low frequencies, $\omega \tau_{\rm br} \ll 1$, the leading order term of $F(\beta)$ in Eq. (9) is equal to $2\pi^{1/2}(\tau_{\rm br}/\tau_{\rm rep})^{1/2} \ll 1$ and the leading order expansion of the expression for the dynamic modulus, Eq. (8), becomes:

$$\frac{G^{*}(\omega)}{G_{\rm e}} = \frac{i\omega \left(\tau_{\rm br}\tau_{\rm rep}\right)^{1/2} / \left(2\pi^{1/2}\right)}{1 + i\omega \left(\tau_{\rm br}\tau_{\rm rep}\right)^{1/2} / \left(2\pi^{1/2}\right)}$$
(10)

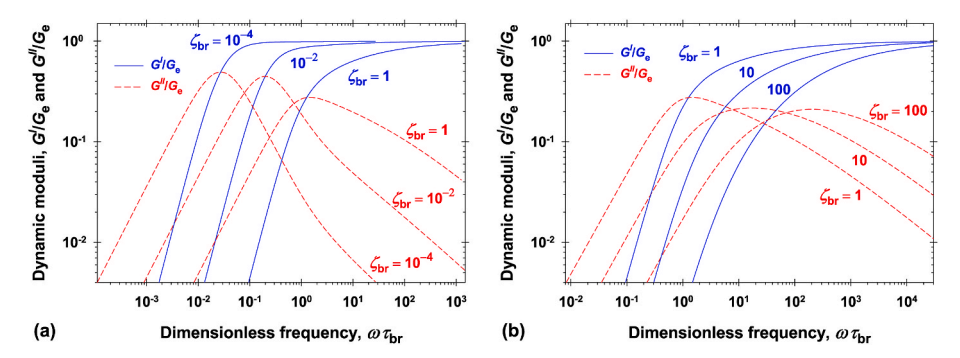


Fig. 2. Dependencies of the dimensionless storage, G'/G_e , and loss, G''/G_e , moduli on the dimensionless frequency, $\omega \tau_{\rm br}$, for different values of $\zeta_{\rm br}$: a) $\zeta_{\rm br} \leq 1$; b) $1 \leq \zeta_{\rm br} \leq 100$.

Note that Eq. (10) has the same form as Eq. (1), which corresponds to the Maxwell model with parameters $G_{\rm M}=G_{\rm e}$ and $\tau_{\rm R}=(\tau_{\rm br}\tau_{\rm rep})^{1/2}/(2\pi^{1/2})=0.282095(\tau_{\rm br}\tau_{\rm rep})^{1/2}$.

The numerical results for the dimensionless storage, G'/G_e , and loss, G''/G_e , moduli calculated from Eqs. (8) and (9) up to large values of ζ_{br} < 100 are summarized in Fig. 2, see also Figs. 1 and 2 in Ref. [29]. The general properties of the PRM and SFM are well illustrated. As it should be: $G'(\omega)$ monotonically increases with the rise of the frequencies of oscillations and $G' \to G_e$ at large values of ω ; $G''(\omega)$ increases to its maximum and subsequently vanishes to zero for large frequencies of oscillations; the $G'(\omega)$ and $G''(\omega)$ curves intersect in the crossover frequency, $\omega_{\rm c}(\tau_{\rm br},\tau_{\rm rep})$, which depends on the mean breaking and the characteristic reptation times. The dynamic modulus at ω_c is denoted by $G_c \equiv G'(\omega_c) = G''(\omega_c)$. Fig. 2 shows that the position of the dimensionless crossover frequency, $\omega_c \tau_{br}$, shifts to the right with the increase of the ratio between the breaking and reptation times, ζ_{br} . It is important to note, that for $\zeta_{\rm br} < 1$, $G''(\omega)$ has a maximum value of $G_{\rm c}$ exactly at $\omega = \omega_{\rm c}$, while for $\zeta_{\rm br} > 1$, the maximum of $G''(\omega)$ is greater than $G_{\rm c}$ and it takes place for frequencies larger than ω_c .

One possible representation of the experimental data is to use the Cole-Cole like plot thus eliminating the frequency information. In the case of Maxwell model, $2G''(\omega)/G_M$ vs $2G'(\omega)/G_M$ is a perfect semicircle and $2G''(1/\tau_R)/G_M=2G'(1/\tau_R)/G_M=1$, see Eq. (1) and Fig. 3. For both PRM and SFM, the corresponding plot can be defined as $G''(\omega)/G_c$ vs $G'(\omega)/G_c$ because of $G''(\omega_c)/G_c=G'(\omega_c)/G_c=1$ (see Fig. 3). One sees that the curves for $\zeta_{br}>1$ deviate considerably from the semicircle even for $G'(\omega)/G_c<1$ and the respective deviations become more pronounced with the increase of ζ_{br} . In the opposite case, $\zeta_{br}<1$, there are parts of the curves (at least for $G'(\omega)/G_c\leq1$, that is for $\omega\leq\omega_c$) that practically lie on the semicircle. Thus, along these parts of the curves, the rheological behavior of the studied WMS corresponds to the Maxwell model of viscoelastic body with an elasticity $G_M=2G_c$ and a relaxation time $\tau_R=1/\omega_c$.

The values of the crossover frequency, ω_c , the dynamic modulus, G_c , and the shear modulus, G_e , are related to the average micelle total contour length, the persistence and entanglement micellar lengths, and the mesh size of the formed network [43]. Thus, their precise experimental observation is important for characterization of the interrelation between the rheology and structure of linear WMSs. In the literature [20–30], the crossover frequency, ω_c , is scaled as $1/\omega_c \propto (\tau_{\rm br} \tau_{\rm rep})^{1/2}$, see Eq. (10). The obtained results (see Appendix S5), calculated numerically here with a relative precision of 10^{-12} , for the dependence of the dimensionless crossover frequency on $\zeta_{\rm br} \leq 100$ are summarized in Fig. 4a (dashed line).

On the other hand, having in mind the cases when one wishes to avoid extensive computational work, we interpolated the numerical data in Fig. 4a using the following empirical relationship:

$$\begin{split} &\omega_{\rm c} \frac{\left(\tau_{\rm br}\tau_{\rm rep}\right)^{1/2}}{2\pi^{1/2}} = \omega_{\rm c}\tau_{\rm rep} \frac{\zeta_{\rm br}^{1/2}}{2\pi^{1/2}} = 1 - 1.20025\zeta_{\rm br}^{1/6} + 0.563515\zeta_{\rm br}^{1/3} \\ &- 0.011221\zeta_{\rm br}^{1/2} \end{split} \tag{11}$$

The solid line in Fig. 4a is drawn using Eq. (11). The relative errors of the interpolated values are less than 1.3 % for all studied ratios between the mean breaking and the characteristic reptation times, $\zeta_{\rm br}$. The respective calculations for the dimensionless dynamic moduli, $2G_{\rm c}/G_{\rm e}$, vs $\zeta_{\rm br}$ are shown in Fig. 4b (dashed line). It is interesting that the curve has a sigmoidal form and the calculated data can be interpolated as follows:

$$\frac{2G_{\rm c}}{G_{\rm e}}\!=\!0.324679+\left[1.47925+0.00152821\exp\!\left(7.61145\zeta_{\rm br}^{1/12}\right)\right]^{-1} \tag{12}$$

The relative errors of the interpolated values are less than 1.4 % for $\zeta_{\rm br} < 100$ (solid line in Fig. 4b).

The representation shown in Fig. 4c can be used for the express estimation of the value of ζ_{br} from the experimental data. The dashed line therein corresponds to the high precision numerical results for $\zeta_{br} \leq 100$ and the solid line is calculated from the following interpolation formula:

$$\zeta_{\rm br} = \frac{(1-\varphi)^2}{\varphi - 0.321784} \left\{ 0.22272 + 1.63381 \right. \\
\left. \left. \left[1 + 1.738214 \frac{(\varphi - 0.321784)^{1.107085}}{(1-\varphi)^{0.369025}} \right]^{1.595659} \right\}$$
(13)

where $\varphi\equiv 2G_c/G_e$. The relative errors of the interpolated values of ζ_{br} are less than 1.4 % for all values of the dimensionless dynamic moduli, $2G_c/G_e$, corresponding to $\zeta_{br}\leq 100$. For example, one estimates the plateau value of the storage modulus at high frequencies of oscillations and the modulus at the crossover point in order to calculate the approximate value of $\varphi=2G_c/G_e$. From interpolation formula, Eq. (13), one calculates the ratio between both characteristic times, ζ_{br} . Subsequently, the dimensionless crossover frequency corresponding to ζ_{br} is calculated from Eq. (11). From ζ_{br} and the experimental value of the crossover frequency, ω_c , the approximate value of the reptation time is obtained. Note that the estimated parameters are not precise but they can be served as an initial guess for the numerical algorithms used to fit the experimental data from oscillatory rheological tests. From our knowledge, the dependencies illustrated in Fig. 4 for $\zeta_{br}\leq 100$ are not published in the literature.

Note that the most experimentalists associate $2G_c$ with the Maxwell elasticity, G_M , see Sections 4 and 5. The shear modulus of the WMS predicted by both PRM and SFM, G_e , is greater than G_M . For example,

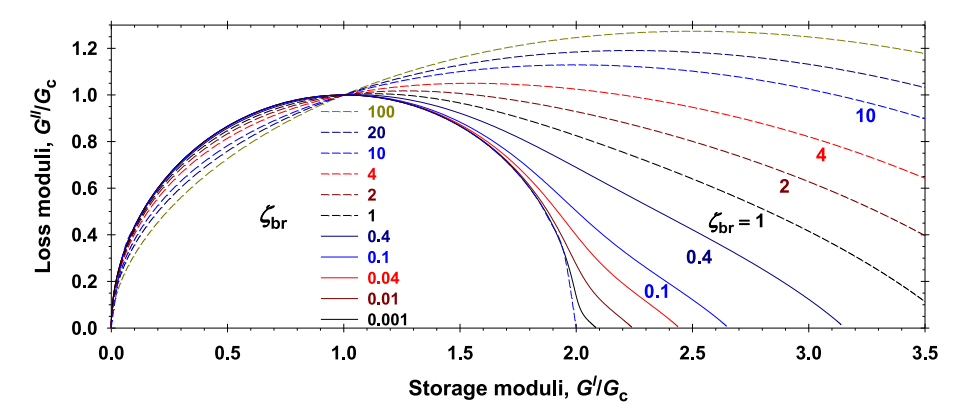


Fig. 3. Cole-Cole like plots: dependencies of the dimensionless loss moduli, G'/G_c , on the dimensionless storage moduli, G'/G_c , for different values of $\zeta_{\rm br} \leq 100$. The perfect semicircle corresponds to the Maxwell model, $2G''/G_{\rm M}$ vs $2G'/G_{\rm M}$.

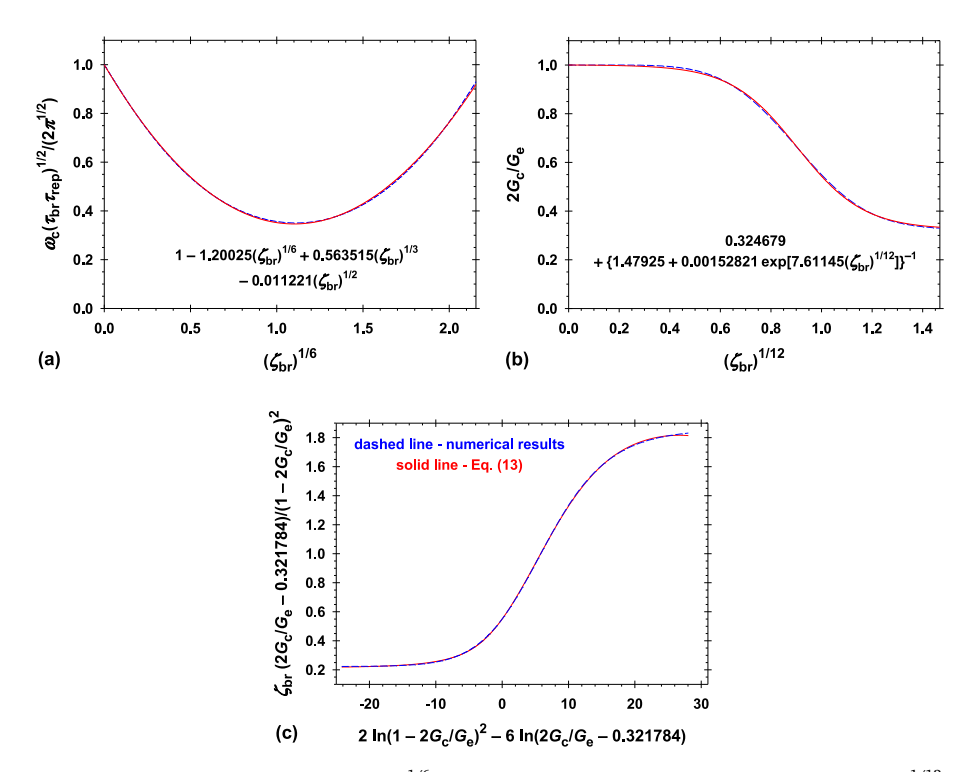


Fig. 4. Dependence of: a) the dimensionless crossover frequency on $(\zeta_{\rm br})^{1/6}$; b) the dimensionless dynamic modulus, $2G_{\rm c}/G_{\rm e}$, on $(\zeta_{\rm br})^{1/12}$; c) $\zeta_{\rm br}$ vs $2G_{\rm c}/G_{\rm e}$. The shown expressions interpolate the numerical values with relative precision lower than 1.4 % for all values of $\zeta_{\rm br} \leq 100$.

 $G_{\rm e}/(2G_{\rm c})=1.82$ for $\zeta_{\rm br}=1$ (Fig. 4b), and the effective Maxwell elasticity, $G_{\rm M}=2G_{\rm c}$, is about two times lower than $G_{\rm e}$. Even for $\zeta_{\rm br}=0.1$, the calculated value is $G_{\rm e}/(2G_{\rm c})=1.328$ and the shear modulus, $G_{\rm e}$, is more than 30 % higher than $G_{\rm M}$. The calculated dependencies shown in Fig. 4 are valid only in the framework of the considered versions of the PRM and SFM. The location of the crossover frequency will change if, for example, contour length fluctuations or end-attack processes are included in the models.

4. Comparison of the results from the data processing of rheological data for WMSs

Fig. 5 summarizes the experimental data for the apparent viscosity, $\eta_{\rm app}$ (the steady shear stress divided by the rate of shear strain), vs the shear rate. At low shear rates, ${\rm d}\gamma/{\rm d}t$, the quasi-Newtonian rheological behavior with a constant zero-shear viscosity, η_0 , is observed for all WMSs. The larger the zero-shear viscosities, the lower the thresholds of the shear rates at which the shear thinning occurs are. At high shear

rates, η_{app} is inversely proportional to $d\gamma/dt$, which is typical for a shear thinning rheological behavior of the WMS [13,15,16,18,19,44].

The zero-shear viscosity increases about 100 times for 12 wt% WMS containing SDS if one replaces the zwitterionic surfactant DDAO with CAPB (Fig. 5). Even at higher surfactant concentrations, the replacement of SDS with C₁₆SME in CAPB containing WMS leads to lower values of η_0 . The relative experimental errors of the measured zero-shear viscosity in each particular run were not higher than 1 %. The mean values of η_0 listed in Table 1 were obtained from the particular values of the zero-shear viscosity measured at least three times starting with newly prepared solutions. Note, that the errors shown in Table 1 correspond to the reproducibility of the experiments. This steady-state rheological regime does not provide information on the elasticity of the micellar solutions.

One way to characterize elasticity $G_{\rm M}$ and viscosity η_0 of viscoelastic Maxwell bodies [43,45] is to apply shear deformations with constant rates of shear strains, ${\rm d}\gamma/{\rm d}t$ (Figs. 1 and 6). The dependence of the shear stress, $\sigma(t)$, on time t obeys the simple exponential law given by Eq. (1). The obtained parameters of the Maxwell model for 15 wt% (1:3)

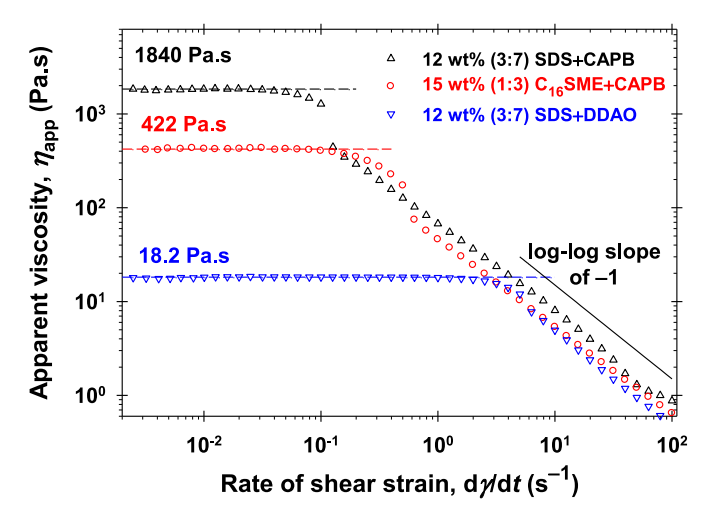


Fig. 5. Dependencies of the apparent viscosity on the rate of shear strain, $d\gamma/dt$, measured for the studied WMSs.

 Table 1

 Rheological parameters of the studied linear wormlike micellar solutions.

System	η_0^a (Pa·s)	$\eta_0^{\ b}$ (Pa·s)	$\eta_0^{\rm c}$ (Pa·s)	G _M ^b (Pa)	2G _c ^c (Pa)
$C_{16}SME + CAPB$	423 ± 5	427 ± 5	425 ± 5	124 ± 4	128 ± 4
$\begin{array}{c} SDS + DDAO \\ SDS + CAPB \end{array}$	$\begin{array}{c} 18.5\pm0.7 \\ 1800\pm50 \end{array}$	$17.9\pm0.6\\1840\pm50$	$18.9\pm0.8\\1750\pm60$	$\begin{array}{c} 142\pm 6 \\ 198\pm 5 \end{array}$	$\begin{array}{c} 148 \pm 4 \\ 202 \pm 5 \end{array}$

- a) Apparent viscosities vs shear rates experiments.
- b) Shear stresses vs shear strains for constant rate of strain experiments.
- c) Oscillatory regimes for small amplitudes of shear strains.

 $C_{16}SME+CAPB$ WMS are given in Section 2, where the relaxation time is $\tau_R=3.42$ s (Fig. 1). The respective results for the particular runs illustrated in Fig. 6 are: a) $G_M=143\pm0.5$ Pa, $\eta_0=17.8\pm0.4$ Pa s, regression coefficient of 0.9995, $d\gamma/dt=0.0979\pm0.0001$ s⁻¹, and $\tau_R=0.124$ s for 12 wt% (3:7) SDS + DDAO WMS; b) $G_M=199\pm0.4$ Pa, $\eta_0=1830\pm5$ Pa s, regression coefficient of 0.9997, $d\gamma/dt=0.0983\pm0.0001$ s⁻¹, and $\tau_R=9.20$ s for 12 wt% (3:7) SDS + CAPB WMS. It is obvious, that the relaxation of the shear stress is the fastest for SDS + DDAO WMS (Fig. 6a) and the slowest for SDS + CAPB WMS (Fig. 6b) because of the about eighty times difference between the relaxation times. The respective parameters with their reproducibility errors listed in Table 1 show that the obtained viscosities, η_0 , from both rheological regimes coincide for each WMS in the frame of the experimental error.

The experimental data for the dynamic storage and loss moduli, G' and G'', vs the frequencies of oscillations, ω , are summarized in Fig. 7 (symbols). The solid lines in Fig. 7 show the best fit results using Eqs. (7) and (8) with adjustable parameters $G_{\rm e}$, $\tau_{\rm br}$, and $\tau_{\rm rep}=\pi^2\tau_{\rm d0}$. In all cases, the regression coefficients were larger than 0.9995 and the theoretical

predictions excellently describe experimental data. The obtained best fit values of the parameters for 15 wt% (1:3) $C_{16}SME + CAPB$ WMS (Fig. 7a) are: $G_e = 224 \pm 1$ Pa, $\tau_{br} = 3.89 \pm 0.02$ s, $\tau_{rep} = 4.73 \pm 0.03$ s. Thus, $\zeta_{br} = 0.822 < 1$ and the rheological response for low frequencies should be close to that of the Maxwell model with $G_M = 2G_c$ and $\tau_R = 1/\omega_c$ (see Fig. 3). Using the calculations shown in Fig. 4, one obtains $G_M = 127$ Pa and $\tau_R = 3.36$ s, so that $\eta_0 = 426$ Pa·s (see dashed lines in Fig. 7a).

It is remarkable that the value of $G_{\rm M}\tau_{\rm R}$ determined from the data in oscillatory regime is in excellent agreement with the values of η_0 independently obtained from the plateau of the respective flow curve in Fig. 5. Such coincidence is sometimes cited as fulfillment of the Cox-Merz rule [46]. This agreement is an argument in favor of the correctness and self-consistence of the used procedure for comparison of theory and experiment. As can be expected, the deviations of the experimental data from the dashed lines are small below the crossover frequency and they are not negligible for $\omega > \omega_{\rm c}$. Note, that the elasticities and viscosities obtained from the all applied rheological regimes coincide in the frame of the reproducibility errors (Table 1). Nevertheless, the shear modulus of the WMS, $G_{\rm ev}$ is 1.76 times larger than elasticity $G_{\rm M}$.

The experimental data for G' and G'' in the case of 12 wt% (3:7) SDS + DDAO WMS are plotted in Fig. 7b. Because of the shorter relaxation time compared to that of 15 wt% (1:3) $C_{16}SME + CAPB$ WMS, the crossover frequency is shifted to the larger values. The respective parameters of the best fit with both PRM and SFM are: $G_e = 259 \pm 2$ Pa, $\tau_{br} = 0.141 \pm 0.003$ s, $\tau_{rep} = 0.193 \pm 0.002$ s (solid lines in Fig. 7b). Note that shear modulus G_e and $\zeta_{br} = 0.729$ have close values to the previous WMS (Fig. 7a), but the mean breaking and characteristic reptation times are more than 25 times lower. As a result, $G_M = 149$ Pa is close to that for 15 wt% (1:3) $C_{16}SME + CAPB$ WMS but $\tau_R = 0.128$ s and $\eta_0 = 19.1$ Pa·s have considerably lower values. Again, G_M is about 1.74 times lower than G_e . The dashed lines corresponding to the Maxwell model in Fig. 7b deviate from experiments at $\omega > \omega_c$.

For 12 wt% (3:7) SDS + CAPB WMS, the best fit parameters of both PRM and SFM are: $G_e = 231 \pm 3$ Pa, $\tau_{br} = 1.89 \pm 0.04$ s, $\tau_{rep} = 145 \pm 5$ s (solid lines in Fig. 7c). As a result, $\zeta_{br} = 1.30 \times 10^{-2}$ and the deviations from the Maxwell model with $G_M = 2G_c = 203$ Pa, $\tau_R = 1/\omega_c = 8.54$ s, and $\eta_0 = 2G_c/\omega_c = 1734$ Pa·s take place for frequencies larger than 0.2 rad/s (Fig. 7c). The difference between G_e and G_M is less than 10 % because of the small values of ζ_{br} . The applied three different rheological regimes give the same values for the respective rheological parameters in the range of reproducibility errors (Table 1).

Fig. 8a summarizes the plots of the experimental loss moduli vs storage moduli for all studied WMSs. This plot is quantitative but it is difficult to compare the different WMSs with respect to their Maxwellian rheological behavior. The Cole-Cole plots represent the dependencies of the dimensionless loss moduli, $2G'/G_{\rm M}$, on the dimensionless storage moduli, $2G'/G_{\rm M}$, where $G_{\rm M}=2G_{\rm C}$ (Figs. 3 and 8b). The region in which the modeling of the WMS like an equivalent Maxwellian viscoelastic body is well illustrated (Fig. 8b) – the lower $\zeta_{\rm br}$, the lower the deviations of experiments from the semicircle are.

In the literature [30,43,45,47], the mesh size of the wormlike micellar solutions, ξ , is related to the shear elasticity, G_e , through the

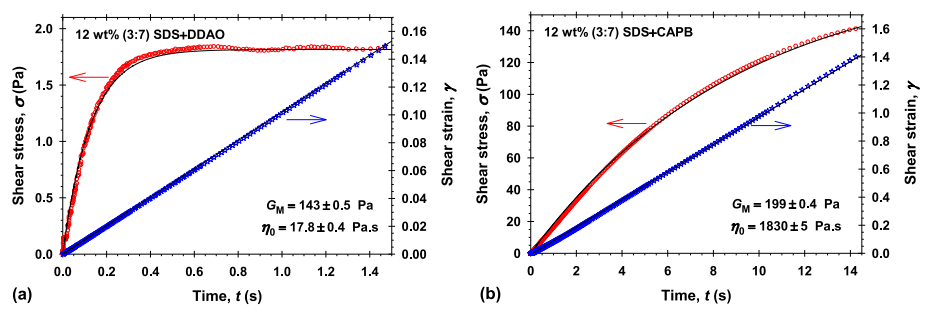


Fig. 6. Dependence of shear strain $\gamma(t)$ and shear stress $\sigma(t)$ on time t, measured for WMS: a) 12 wt% (3:7) SDS + DDAO; b) 12 wt% (3:7) SDS + CAPB.

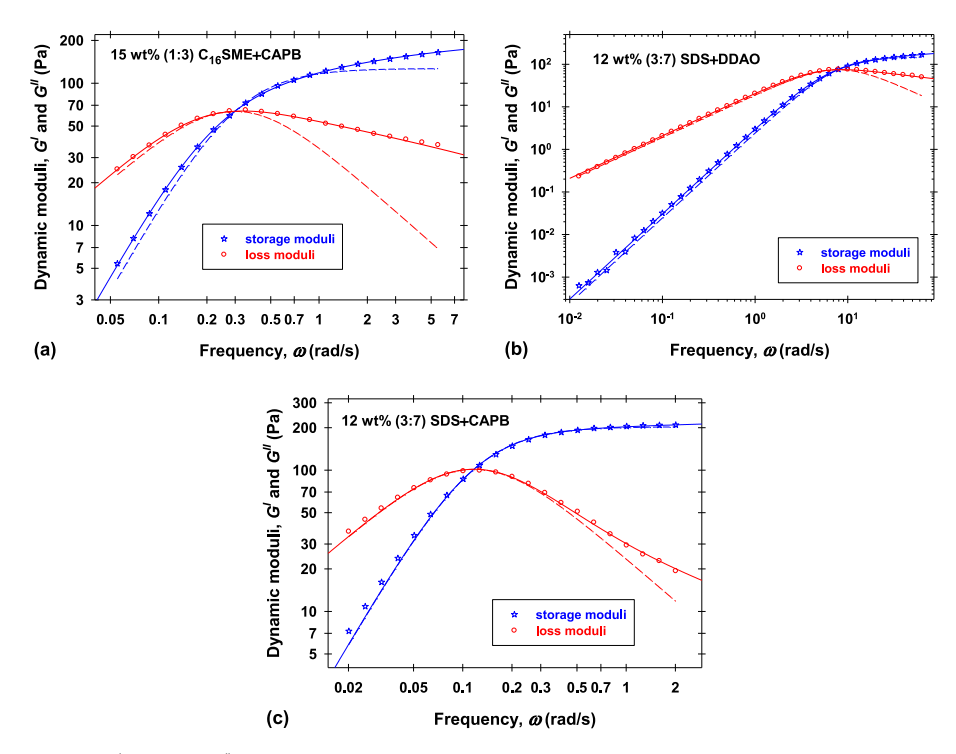


Fig. 7. Dependencies of the storage, G', and loss, G'', moduli on the frequency of oscillations, ω , for the studied WMSs: a) 15 wt% (1:3) $C_{16}SME + CAPB$; b) 12 wt% (3:7) SDS + DDAO; c) 12 wt% (3:7) SDS + CAPB. The symbols represent the experimental data, the solid lines show the best fit results from both PRM and SFM, and the dashed lines correspond to the Maxwell model with parameters calculated at the crossover points.

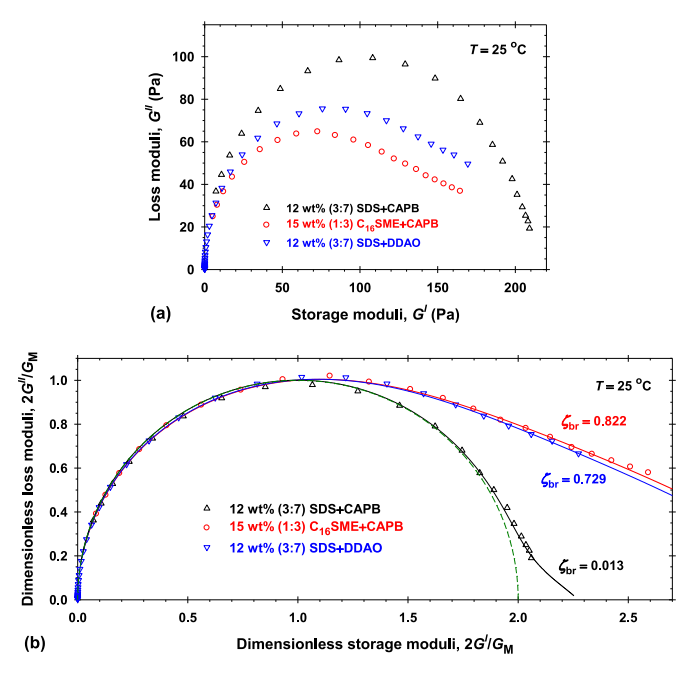


Fig. 8. a) Dependencies of loss moduli G'' on storage moduli G'' for the studied WMSs; b) Cole-Cole plots – dependencies of the dimensionless loss moduli, $2G'/G_{M}$, on the dimensionless storage moduli, $2G'/G_{M}$, where $G_{M}=2G_{c}$. The solid lines are the best theoretical fits according to Eqs. (7) and (8), the symbols show the experimental data.

following expression, $\xi = (Ak_{\rm B}T/G_{\rm e})^{1/3}$, where $k_{\rm B}$ is the Boltzmann constant, T is the absolute temperature, and the prefactor A is theoretically derived from correlations for entangled polymers to be equal to 9.75. For the studied WMSs, the calculated values of the mesh size are: 42 nm for 15 wt% (1:3) $C_{16}SME + CAPB$; 40 nm for 12 wt% (3:7) SDS + DDAO; 41 nm for 12 wt% (3:7) SDS + CAPB. These values are approximately equal (\approx 40 nm) because of the comparable micellar volume

fractions. In contrast, if one uses the obtained values of $G_{\rm M}$ (Table 1) instead of $G_{\rm e}$, then one calculates 48 nm for SDS + DDAO and 43 nm for SDS + CAPB, which are different for equal micellar volume fractions.

These results show that if one wants to obtain the structural parameters of the WMS (the average wormlike micelle length, the persistence and entanglement lengths, and the mesh size of the formed network), then one needs to process rheological data for the dynamic

Table 2Rheological parameters obtained from the PRM for the studied linear wormlike micellar solutions.

System	G _e (Pa)	τ_{rep} (s)	τ_{br} (s)	$\tau_{\rm B0}^{\rm a}$ (s)	$\tau_{\rm B0}^{\rm \ b}$ (s)
$C_{16}SME + CAPB$	$\textbf{224} \pm \textbf{1}$	4.73 ± 0.03	3.89 ± 0.02	6.89 ± 0.03	4.67 ± 0.02
SDS + DDAO	259 ± 2	0.193 ± 0.002	0.141 ± 0.003	0.247 ± 0.004	0.168 ± 0.003
SDS + CAPB	231 ± 3	145 ± 5	1.89 ± 0.04	2.77 ± 0.05	1.78 ± 0.04

a) Eq. (6a) is used for the dependence of τ_B on τ_{B0} and z.

moduli using the PRM or the SFM in order to calculate precisely the physical elasticity, $G_{\rm e}$, the mean breaking, $\tau_{\rm br}$, and the characteristic reptation, $\tau_{\rm rep}$, times.

5. Discussions on the rheological models

In the original PRM [27], the breaking time, $\tau_B(z)$, depends on the length of wormlike micelles, see Eqs. (6a) and (6b), and there are no closed-form analytical expressions for G' and G''. The simpler SFM and PRM with constant breaking time $\tau_B(z) = \tau_{\rm br}$ excellently describe the experimental data. It is important to show the possibility to use rheological experiments to distinguish the length-dependence PRM models with the SFM. For that reason, we fixed the values of the shear elastic moduli, $G_{\rm e}$, and the characteristic reptation times, $\tau_{\rm rep}$, obtained from the SFM (see Table 2) and varied only the characteristic breaking time, $\tau_{\rm B0}$, appearing in Eqs. (6a) and (6b). The storage and loss moduli, G' and G'', were calculated from the general relationship, Eq. (7), using the respective complex numerical integrations, see Eqs. (S9) and (S10), applying a high precision numerical algorithm.

The obtained parameters from the best fits with one adjustable parameter, τ_{B0} , are listed in Table 2 for the particular cases of WMSs. In all cases, the regression coefficients were greater than 0.9995. Fig. S2 summarizes the dependencies of the dimensionless storage, G'/G_e , and loss, G''/G_e , moduli on the frequency of oscillations, ω , calculated using the rheological parameters given in Table 2. It is impressive, that the models with constant $\tau_{\rm br}$ and length-dependent $\tau_{\rm B}(z)$ predict practically the same dependencies of the dynamic moduli on frequency ω . Thus, the breaking time models cannot be distinguished based on the concrete experimental data. The differences are only in the values of the mean, $\tau_{\rm br}$, and the characteristic, $\tau_{\rm B0}$, breaking times.

To check the generality of this conclusion, we have chosen the following strategy. First, one calculates the value of the crossover frequency, $\omega_{\rm c}(\tau_{\rm br},\tau_{\rm rep})$, predicted from the SFM, for given breaking and reptation times, $\tau_{\rm br}$ and $\tau_{\rm rep}$. Second, one varies $\tau_{\rm B0}$ in the general PRM with length-dependent $\tau_{\rm B}(z)$ to obtain the same crossover frequency, $\omega_{\rm c}(\tau_{\rm br},\tau_{\rm rep})$, for the same reptation time, $\tau_{\rm rep}$. Thus, the ratio between the obtained characteristic breaking times, $\tau_{\rm B0}/\tau_{\rm br}$, becomes a universal function only of $\zeta_{\rm br}$.

Fig. 9a and S1 show the comparisons between the PRM using the

constant value of the breaking time, $\tau_{\rm br}$, and $\tau_{\rm B}(z)$ calculated from Eqs. (6a) and (6b) for different ratios $\zeta_{\rm br}$ from 0.01 to 100. Solid lines correspond to the numerical solution from the PRM with constant $\tau_{\rm B}(z) = \tau_{\rm br}$; circles show the results from the PRM in the case of reversible scission rearrangements, $\tau_{\rm B}(z)$ is calculated from Eq. (6a); stars – when the linear wormlike micelles rearrange by the end attack pathway, $\tau_{\rm B}(z)$ is given by Eq. (6b). One sees that the models with constant $\tau_{\rm br}$ and length-dependent $\tau_{\rm B}(z)$ predict practically the same dependencies of the dimensionless storage, $G'/G_{\rm e}$, and loss, $G''/G_{\rm e}$, moduli on the dimensionless frequency, $\omega\tau_{\rm br}$.

The dashed lines in Fig. 9b show the obtained dependencies of τ_{B0}/τ_{br} on ζ_{br} calculated from both length-dependent variants of the PRM. One sees that $1.41 < \tau_{B0}/\tau_{br} < 2.02$ in the case of reversible scission rearrangements and $0.891 < \tau_{B0}/\tau_{br} < 1.41$ when the wormlike micelles rearrange by the end attack pathway. In both cases, τ_{B0}/τ_{br} monotonically increases with the increase of ζ_{br} . The universal curves in Fig. 9b have sigmoidal forms and for express calculations, these dependencies can be interpolated as follows:

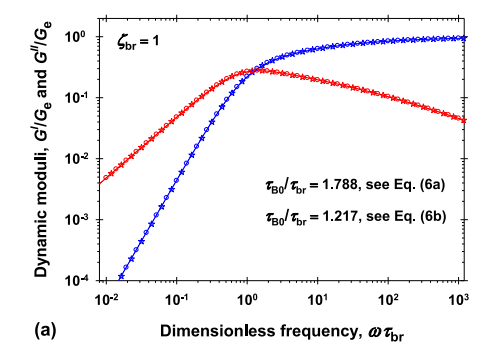
a) for reversible scission rearrangements, $\tau_B(z)$ is defined by Eq. (6a) and the interpolation formula reads:

$$\frac{\tau_{B0}}{\tau_{hr}} = 1.4113 + \left[1.6502 + 8031.2 \exp\left(-8.9990\zeta_{hr}^{1/12}\right)\right]^{-1}$$
 (14a)

b) when the linear wormlike micelles rearrange by the end attack pathway, $\tau_B(z)$ is given by Eq. (6b) and the interpolation expression is:

$$\frac{\tau_{B0}}{\tau_{br}} = 0.89127 + \left[1.9094 + 8982.5 \exp\left(-8.9700\zeta_{br}^{1/12}\right)\right]^{-1}$$
 (14b)

The relative errors of both interpolation formulae (solid lines in Fig. 9b) are less than 1 % for $\zeta_{br} \leq$ 100. Thus, one can process rheological experimental data using the exact expressions for the simpler SFM, Eqs. (7) and (8), to obtain G_e , τ_{br} , and τ_{rep} , and subsequently to calculate τ_{B0} from the interpolation formulae, Eq. (14a) or Eq. (14b). Using this approach, the numerical problems with the integration of functions of complex variables and the precision of the numerical procedures are avoided and the time of calculation is considerably accelerated.



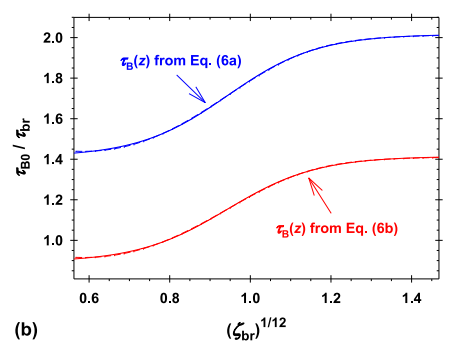


Fig. 9. a) Dependencies of the dimensionless storage, G'/G_e , and loss, G''/G_e , moduli on the dimensionless frequency, $\omega \tau_{br}$, for $\zeta_{br}=1$. Solid lines correspond to the numerical solution from the PRM with constant $\tau_B(z)=\tau_{br}$; circles show the results from the PRM with $\tau_B(z)$ calculated from Eq. (6a) for $\tau_{B0}/\tau_{br}=1.788$; stars – the results from the PRM with $\tau_B(z)$ calculated from Eq. (6b) for $\tau_{B0}/\tau_{br}=1.217$. b) τ_{B0}/τ_{br} vs ζ_{br} – dashed lines show the numerical results and solid lines correspond to the interpolation formulae given by Eqs. (14a)–(14b).

b) $\tau_{\rm B}(z)$ is calculated from Eq. (6b).

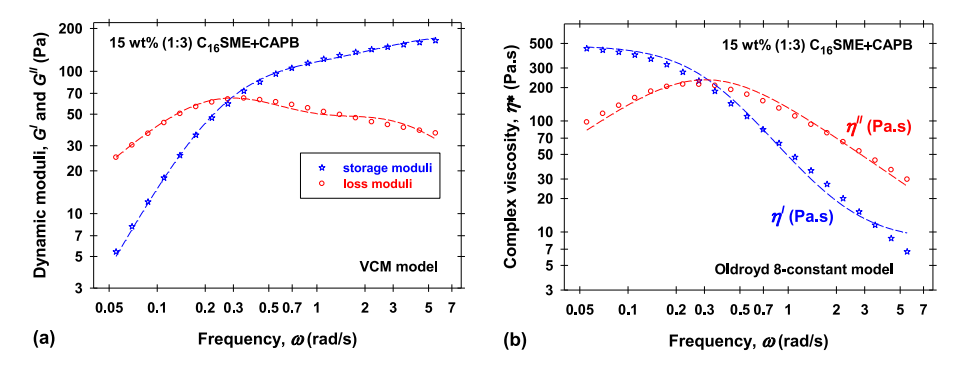


Fig. 10. a) Dependencies of the storage, G', and loss, G'', moduli on the frequency, ω, for 15 wt% (1:3) $C_{16}SME + CAPB$ WMS. Dashed lines correspond to the best fit results using the VCM model with parameters listed in Table S1 b) Dependencies of the loss, η', and storage, η'', viscosities on the frequency, ω, for 15 wt% (1:3) $C_{16}SME + CAPB$ WMS. Dashed lines correspond to the best fit results using the single-mode Oldroyd 8-constant model with parameters listed in Table S2.

Table 3 Limiting elasticity, $G'(\infty)$, and viscosity allow shear rates, $\eta(0)$, predicted from the VCM and the single-mode Oldroyd 8-constant models for studied WMSs.

System	VCM model [37–39]		Oldroyd 8-constant model [40]		
	<i>G</i> ′(∞) (Pa)	η(0) (Pa·s)	$G'(\infty)$ (Pa)	η(0) (Pa·s)	
$C_{16}SME + CAPB$	186 ± 10	469 ± 5	143 ± 6	479 ± 4	
SDS + DDAO	197 ± 8	21.0 ± 0.3	144 ± 4	21.7 ± 0.3	
SDS + CAPB	217 ± 12	1840 ± 40	208 ± 8	1840 ± 50	

Both PRM and SFM have a clear physicochemical meaning and allow relating the WMS rheology and bulk structure. Nevertheless, they are not applicable for engineering calculations: there is not a known corresponding theoretical relationship between the total stress tensor, strain tensor and their rates, which represents the general rheological constitutive relationship in the non-Newtonian hydrodynamic of complex fluids. Peterson and Cates [48] have shown that additional approximations must be made with respect to reptation and constraint release in order to facilitate applications in computational fluid dynamics. As a result, it is not possible to model the flows in tubes and reservoirs, hydrodynamic resistances, filling and pumping, etc. of WMSs with the use of the PRM and SFM predictions. For that reason, recent rheological models having tensorial representations and postulating hydrodynamic constitutive rheological relationships are developed in the literature. The most popular are: a) the Vasquez-Cook-McKinley model [37-39]; b) different versions of the Oldroyd 8-constant model [40].

The two species Vasquez-Cook-McKinley model (VCM model) [37–39] considers two elastically active Hookean species: long chains which can break to form two short chains, which can themselves recombine to form a long chain. In the linear viscoelastic regime, the VCM model expressions for the storage and loss moduli are given by Eqs. (S38a) and (S38b). The best theoretical lines calculated using the VCM model are shown in Fig. 10a and S3 and the values of the best fit model parameters are listed in Table S1. For all studied WMSs the regression coefficients are larger than 0.9996 and the description of the experimental data is good. The calculated best fit values of the elastic moduli at high frequencies, $G'(\infty)$, and the viscosity allow shear rates, $\eta(0)$, are listed in Table 3. Note, that $\eta(0)$ has a meaning of the zero-shear viscosity, η_0 , and $G'(\infty)$ – of the shear modulus, G_e , of the WMSs. It is obvious, that the VCM model predicts the zero-shear viscosity with better precision (c.f. Tables 1 and 3) compared to the shear modulus (c.f. Tables 2 and 3).

For the single-mode Oldroyd 8-constant framework, the dependencies of the complex, η^* , loss, $\eta' \equiv G'/\omega$, and storage, $\eta'' \equiv G'/\omega$, viscosities on frequency ω are calculated from Eq. (S41). Fig. 10b and S4 show that the best theoretical lines (dashed lines), calculated with parameters given in Table S2, describe well all experimental data with the

values of the regression coefficients greater than 0.998. As should be, the predicted values of the viscosity at low shear rates, $\eta(0)$, are close to the zero-shear viscosity, η_0 , see Tables 1 and 3. It is important to note, that the best fit values of the limiting elasticity, $G'(\infty)$, given in Table 3 are systematically lower than the shear modulus, G_e , of all studied WMSs: $G'(\infty)$ are close to the elasticities corresponding to the Maxwell model summarized in Table 1.

6. Conclusions

The shear rheology of linear wormlike micellar solutions (WMSs) at low and intermediate rates of shear strains is well described by both Poisson renewal (PRM) [27] and shuffling (SFM) [29,36] models using the system parameters: shear elasticity, $G_{\rm e}$; characteristic reptation time, $\tau_{\rm rep}$; mean breaking time, $\tau_{\rm br}$. At low values of the shear strains and their rates, the linear WMSs behave as a Maxwellian viscoelastic body with constant elasticity $G_{\rm M}$ and zero-shear viscosity η_0 . The relationships between both sets of experimentally observed parameters ($\{G_{\rm e}, \tau_{\rm rep}, \tau_{\rm br}\}$ and $\{G_{\rm M}, \eta_0\}$) are not well described in the literature.

If the breaking time in the PRM is a constant and the reptation time, τ_{d0} , evaluated with respect to the average chain length is used to define the characteristic reptation time, $\tau_{\rm rep} = \pi^2 \tau_{\rm d0}$, then both PRM and SFM predict identical dependencies of the dynamic modulus, G^* , vs frequency of oscillations ω , Eqs. (9) and (10). The closed analytical form for the Laplace image of the stress relaxation function and the respective infinite series for the complex modulus [36] give possibility for fast and precise calculations and express rheological data processing. The storage, $G'(\omega)$, and loss, $G''(\omega)$, moduli have equal values at the crossover frequency, ω_c , where $G_c = G'(\omega_c) = G''(\omega_c)$. The reported here dependencies of the dimensionless crossover frequency and the ratio between $G_{\rm c}$ and the shear modulus of solution, $G_{\rm e}$, on the ratio $\zeta_{\rm br}=$ $\tau_{\rm br}/\tau_{\rm rep}$, see Fig. 4 and Eqs. (11)–(13), provide information on the parameter of the Maxwell rheological model, $G_{\rm M}=2G_{\rm c}$ and $\eta_0=2G_{\rm c}/\omega_{\rm c}$, and are used to construct the respective normalized Cole-Cole plots, see Figs. 3 and 8b, for all values of $\zeta_{br} \le 100$. Eqs. (11) and (13) can be used for the calculation of the approximate values of τ_{br} and τ_{rep} from experimental data obtained in oscillatory rheological tests. From the viewpoint of experimental data for $G'(\omega)$ and $G''(\omega)$, the micellar-length-dependent breaking-time version of the PRM [27], Eqs. (6a) and (6b), become indistinguishable for the dependencies of τ_{B0}/τ_{br} on ζ_{br} shown in Fig. 9b for all ratios between the mean breaking and characteristic relaxation times ($\zeta_{br} \leq 100$). Thus, one can process experimental data for $G'(\omega)$ and $G''(\omega)$ using the simpler SFM to obtain $G_{\rm e},\, au_{
m br}$, and $au_{
m rep}$, and subsequently to calculate $au_{
m B0}$ from the interpolation formulae, Eq. (14a) or Eq. (14b), avoiding the complex numerical problems with the integration of functions of complex variables.

The experimental data from independent static and dynamic rheological regimes (apparent viscosity vs shear rate, stress vs strain at constant shear rates, strain oscillations at low amplitudes and a wide

range of frequencies) applied to low, medium, and high zero-shear viscosity WMSs are described excellently by the theoretical models (Section 4). They demonstrate the self-consistency of the applied models and point that G_M can be about two times lower than the physical shear elasticity, G_e , for comparable values of the breaking and reptation times.

The physicochemical interpretation of both PRM and SFM allows relating the rheology to the parameters of the wormlike micellar structures but both PRM and SFM have no general tensorial representations and cannot be used for hydrodynamic modeling of non-Newtonian complex fluids. The hydrodynamic constitutive rheological relationships are obtained in the framework of the Vasquez-Cook-McKinley model (VCM) [37-39] and the 8-constant Oldroyd model [40]. These models describe well the viscosity of linear WMSs (Fig. 10, S3, and S4) but the predicted elasticities are systematically lower than the respective shear elasticities, Ge. Regardless of the VCM and the 8-constant Oldroyd models applicability for engineering calculations, they do not provide information on the micellar structures.

The results are useful for a wide auditorium of experimentalists for express and precise interpretation of rheological experiments with WMSs. They put a light on the similarity of both PRM and SFM and the relationships between the physical parameters of the theoretical rheological models.

CRediT authorship contribution statement

Krassimir D. Danov: Writing – original draft, Supervision, Software, Formal analysis. Gergana M. Radulova: Investigation, Data curation. Jordan T. Petkov: Methodology, Conceptualization. Yee Wei Ung: Supervision, Project administration, Funding acquisition, Conceptualization.

Declaration of competing interest

The authors declare that they have no known competing financial interests or personal relationships that could have appeared to influence the work reported in this paper.

Acknowledgements

The authors gratefully acknowledge the support from KLK OLEO. This research was funded by the European Regional Development Fund under the Operational Program "Scientific Research, Innovation and Digitization for Smart Transformation 2021–2027", Project CoC "Smart Mechatronics, Eco- and Energy Saving Systems and Technologies", BG16RFPR002-1.014-0005.

List of symbols and notations

C₁₆SME palmitic sulfonated methyl ester

CAPB cocamidopropyl betaine

DDAO N,N-dimethyldodecylamine N-oxide

G'dynamic storage modulus G''dynamic loss modulus

 $G^* = G' + iG''$ dynamic complex modulus

stress relaxation function

 $G_{\rm c} = G'(\omega_{\rm c}) = G''(\omega_{\rm c})$ dynamic modulus calculated at $\omega_{\rm c}$

 $G_{\rm e}$ shear modulus of solution

Laplace image of G with respect to time $G_{
m L}$

 $G_{\rm M}$ shear elasticity in the Maxwell model of viscoelastic body

chain length L L_{a}

average chain length

Poisson renewal model for wormlike micellar solutions PRM

SDS sodium dodecyl sulfate

shuffling model for wormlike micellar solutions SFM

temperature T

VCM Vasquez-Cook-McKinley model [37-39]. WMS wormlike micellar solution

 $d\gamma/dt$ rate of shear strain Boltzmann constant $k_{\rm B}$

t

 $z = L/L_a$ dimensionless chain length

shear strain $\eta' = G''/\omega$ loss viscosity

 $\eta'' = G'/\omega$ storage viscosity

 $\eta^* = \eta' + i\eta''$ complex viscosity

zero-shear viscosity and viscosity in the Maxwell model of viscoelastic body

 $\varphi = 2G_{\rm c}/G_{\rm e}~$ ratio between dynamic moduli

 $\sigma(t)$ shear stress

characteristic breaking time defined in the length-dependence original version PRM

breaking time defined in the length-dependence original $\tau_{\rm B}(z)$ version of PRM

mean breaking time

 $\tau_{\rm d}(z)$ reptation time of the L-chain

reptation time evaluated with respect to the average chain τ_{d0}

 $\tau_{\rm R} = \eta_0/G_{\rm M}$ relaxation time in the Maxwell model of viscoelastic body

characteristic reptation time $\tau_{\rm rep}$ frequency of oscillations ω

 $\omega_{\rm c}(\tau_{\rm br}, \tau_{\rm rep})$ crossover frequency

mesh size of the wormlike micellar solution

 $\zeta_{\rm br} = \tau_{\rm br}/\tau_{\rm rep}$ ratio between the mean breaking and the characteristic reptation times

Appendix A. Supplementary data

Supplementary data to this article can be found online at https://doi. org/10.1016/j.jciso.2025.100160.

Data availability

Data will be made available on request.

References

- [1] C.A. Dreiss, Wormlike micelles; where do we stand? Recent developments, linear rheology and scattering techniques, Soft Matter 3 (2007) 956-970, https://doi. org/10.1039/B705775J
- [2] G. Porte, R. Gomati, O. El Haitdmy, J. Appell, J. Marignan, Morphological transformations of the primary surfactant structures in brine-rich mixtures of ternary systems (surfactant/alcohol/brine), J. Phys. Chem. 90 (1986) 5746-5751, https://doi.org/10.1021/i100280a055
- [3] T.J. Drye, M.E. Cates, Living networks: the role of cross-links in entangled surfactant solutions, J. Chem. Phys. 96 (1992) 1367-1375, https://doi.org/
- [4] S.J. Candau, A. Khatory, F. Lequeux, F. Kern, Rheological behavior of wormlike micelles: effect of salt content, J. Phys. IV France 3 (1993), https://doi.org/ 10.1051/jp4:1993117. C1-197 – C1-209.
- [5] J. Appell, G. Porte, A. Khatory, F. Kern, S.J. Candau, Static and dynamic properties of a network of wormlike surfactant micelles (cetylpyridinium chlorate in sodium chlorate brine), J. Phys. II France 2 (1992) 1045-1052, https://doi.org/10.1051/
- [6] L. Nicolas-Morgantini, Giant micelles and shampoos, in: R. Zana, E.W. Kaler (Eds.), Giant Micelles. Properties and Applications, Taylor and Francis, New York, 2007, pp. 493-514, https://doi.org/10.1201/9781420007121. Chapter 17.
- S. Ezrahi, E. Tuval, A. Aserin, N. Garti, Daily applications of systems with wormlike micelles, in: R. Zana, E.W. Kaler (Eds.), Giant Micelles. Properties and Applications, Taylor and Francis, New York, 2007, pp. 515-544, https://doi.org/10. 9781420007121. Chapter 18.
- [8] P.F. Sullivan, M.K.R. Panda, V. Laffite, Applications of wormlike micelles in oilfield industry, in: C. Dreiss, Y. Feng (Eds.), Wormlike Micelles. Advances in Systems, Characterization and Applications, RSC, 2017, pp. 330-352, https://doi.org/ 10.1039/9781782629788-00330. Chapter 12.
- [9] J.L. Zakin, A.J. Maxson, T. Saeki, P.F. Sullivan, Turbulent drag-reduction applications of surfactant solutions, in: C. Dreiss, Y. Feng (Eds.), Wormlike Micelles. Advances in Systems, Characterization and Applications, RSC, 2017, pp. 353-378, https://doi.org/10.1039/9781782629788-00353. Chapter 13.

- [10] A. Bernheim-Groswasser, E. Wachtel, Y. Talmon, Micellar growth, network formation, and criticality in aqueous solutions of the nonionic surfactant C₁₂E₅, Langmuir 16 (2000) 4131–4140, https://doi.org/10.1021/la991231q.
- [11] K.D. Danov, P.A. Kralchevsky, S.D. Stoyanov, J.L. Cook, I.P. Stott, E.G. Pelan, Growth of wormlike micelles in nonionic surfactant solutions: quantitative theory vs. experiment, Adv. Colloid Interface Sci. 256 (2018) 1–22, https://doi.org/ 10.1016/j.cis.2018.05.006.
- [12] D.P. Acharya, H. Kunieda, Wormlike micelles in mixed surfactant solutions, Adv. Colloid Interface Sci. 123–126 (2006) 401–413, https://doi.org/10.1016/j. cis.2006.05.024.
- [13] S. Różańska, Rheology of wormlike micelles in mixed solutions of cocoamidopropyl betaine and sodium dodecylbenzenesulfonate, Colloids Surf., A 482 (2015) 394–402, https://doi.org/10.1016/j.colsurfa.2015.06.045.
- [14] K.D. Danov, P.A. Kralchevsky, R.D. Stanimirova, S.D. Stoyanov, J.L. Cook, I. P. Stott, Analytical modelling of micelle growth. 4. Molecular thermodynamics of wormlike micelles from ionic surfactants: theory vs. experiment, J. Colloid Interface Sci. 584 (2021) 561–581, https://doi.org/10.1016/j.jcis.2020.10.004.
- [15] Z. Mitrinova, H. Alexandrov, N. Denkov, S. Tcholakova, Effect of counter-ion on rheological properties of mixed surfactant solutions, Colloids Surf., A 643 (2022) 128746, https://doi.org/10.1016/j.colsurfa.2022.128746.
- [16] Z. Mitrinova, Z. Valkova, S. Tcholakova, Interplay between cosurfactants and electrolytes for worm-like micelles formation, Colloids Surf., A 707 (2025) 135943, https://doi.org/10.1016/j.colsurfa.2024.135943.
- [17] F.B. Bombelli, D. Berti, M. Almgren, G. Carlsson, P. Baglioni, Light scattering and cryo-transmission electron microscopy investigation of the self-assembling behavior of Di-C₁₂P-nucleosides in solution, J. Phys. Chem. B 110 (2006) 17627–17637, https://doi.org/10.1021/jp060594d.
- [18] Z. Mitrinova, S. Tcholakova, N. Denkov, Control of surfactant solution rheology using medium-chain cosurfactants, Colloids Surf., A 537 (2018) 173–184, https://doi.org/10.1016/j.colsurfa.2017.10.018.
- [19] V.I. Yavrukova, G.M. Radulova, K.D. Danov, P.A. Kralchevsky, H. Xu, Y.W. Ung, J. T. Petkov, Rheology of mixed solutions of sulfonated methyl esters and betaine in relation to the growth of giant micelles and shampoo applications, Adv. Colloid Interface Sci. 275 (2020) 102062, https://doi.org/10.1016/j.cis.2019.102062.
- [20] M.E. Cates, Reptation of living polymers: dynamics of entangled polymers in the presence of reversible chain-scission reactions, Macromolecules 20 (1987) 2289–2296, https://doi.org/10.1021/ma00175a038.
- [21] M.E. Cates, Dynamics of living polymers and flexible surfactant micelles: scaling laws for dilution, J. Phys. France 49 (1988) 1593–1600, https://doi.org/10.1051/ jphys:019880049090159300.
- [22] M.E. Cates, Nonlinear viscoelasticity of wormlike micelles (and other reversibly breakable polymers), J. Phys. Chem. 94 (1990) 371–375, https://doi.org/10.1021/ i100364a063
- [23] M.E. Cates, S.J. Candau, Statics and dynamics of worm-like micelles, J. Phys. Condens. Matter 2 (1990) 6869–6892. http://refhub.elsevier.com/S0001-8686 (19)30347-1/rf0110.
- [24] M.S. Turner, M.E. Cates, Linear viscoelasticity of living polymers: a quantitative probe of chemical relaxation times, Langmuir 7 (1991) 1590–1594, https://doi. org/10.1021/la00056a009.
- [25] F. Kern, P. Lemarechal, S.J. Candau, M.E. Cates, Rheological properties of semidilute and concentrated aqueous solutions of cetyltrimethylammonium bromide in the presence of potassium bromide, Langmuir 8 (1992) 437–440, https://doi.org/10.1021/ja00038a020
- [26] M.E. Cates, S.M. Fielding, Rheology of giant micelles, Adv. Phys. 55 (2006) 799–879, https://doi.org/10.1080/00018730601082029.
- [27] R. Granek, M.E. Cates, Stress relaxation in living polymers: results from a poisson renewal model, J. Chem. Phys. 96 (1992) 4758–4767, https://doi.org/10.1063/ 1.465787
- [28] J.D. Peterson, M.E. Cates, A full-chain tube-based constitutive model for living linear polymers, J. Rheol. 64 (2020) 1465–1496, https://doi.org/10.1122/ 8.0000114
- [29] J.D. Peterson, W. Zou, R.G. Larson, M.E. Cates, Wormlike micelles revisited: a comparison of models for linear rheology, J. Non-Newtonian Fluid Mech. 322 (2023) 105149, https://doi.org/10.1016/j.jnnfm.2023.105149.

- [30] W. Zou, R.G. Larson, A mesoscopic simulation method for predicting the rheology of semi-dilute wormlike micellar solutions, J. Rheol. 58 (2014) 681–721, https:// doi.org/10.1122/1.4868875.
- [31] W. Zou, X. Tang, M. Weaver, P. Koenig, R.G. Larson, Determination of characteristic lengths and times for wormlike micelle solutions from rheology using a mesoscopic simulation model, J. Rheol. 59 (2015) 903–934, https://doi.org/ 10.1122/1.4919403.
- [32] Z. Wang, X. Chen, R.G. Larson, Comparing tube models for predicting the linear rheology of branched polymer melts, J. Rheol. 54 (2010) 223–250, https://doi. org/10.1122/1.3301246.
- [33] S.A. Rogers, M.A. Calabrese, N.J. Wagner, Rheology of branched wormlike micelles, Curr. Opin. Colloid Interface Sci. 19 (2014) 530–535, https://doi.org/ 10.1016/j.cocis.2014.10.006
- [34] M.A. Calabrese, S.A. Rogers, R.P. Murphy, N.J. Wagner, The rheology and microstructure of branched micelles under shear, J. Rheol. 59 (2015) 1299–1328, https://doi.org/10.1122/1.4929486.
- [35] W. Zou, G. Tan, M. Weaver, P. Koenig, R.G. Larson, Mesoscopic modeling of the effect of branching on the viscoelasticity of entangled wormlike micellar solutions, Phys. Rev. Res. 5 (2023) 043024, https://doi.org/10.1103/ PhysRevResearch.5.043024.
- [36] V. Chen, C.T. Drucker, C. Love, J. Peterson, J.D. Peterson, Analytical solution for the linear rheology of living polymers, J. Non-Newtonian Fluid Mech. 334 (2024) 105343, https://doi.org/10.1016/j.jnnfm.2024.105343.
- [37] P.A. Vasquez, G.H. McKinley, L.P. Cook, A network scission model for wormlike micellar solutions: I. Model formulation and viscometric flow predictions, J. Non-Newtonian Fluid Mech. 144 (2007) 122–139, https://doi.org/10.1016/j. jnnfm.2007.03.007.
- [38] N. German, L.P. Cook, A.N. Beris, Nonequilibrium thermodynamic modeling of the structure and rheology of concentrated wormlike micellar solutions, J. Non-Newtonian Fluid Mech. 196 (2013) 51–57, https://doi.org/10.1016/j. jnnfm.2012.12.010.
- [39] S. Varchanis, S.J. Haward, C.C. Hopkins, J. Tsamopoulos, A.Q. Shen, Evaluation of constitutive models for shear-banding wormlike micellar solutions in simple and complex flows, J. Non-Newtonian Fluid Mech. 307 (2022) 104855, https://doi. org/10.1016/j.jnnfm.2022.104855.
- [40] C. Saengow, A.J. Giacomin, N. Grizutti, R. Pasquino, Startup steady shear flow from the oldroyd 8-constant framework, Phys. Fluids 31 (2019) 063101, https:// doi.org/10.1063/1.5091493.
- [41] T.G. Slavova, G.M. Radulova, K.D. Danov, Saturated micellar networks: phase separation and nanoemulsification capacity, Colloids Interfaces 8 (2024) 11, https://doi.org/10.3390/colloids8010011.
- [42] M. Doi, S.F. Edwards, The Theory of Polymer Dynamics, Clarendon, Oxford, 1986.
- [43] R. Pasquino, R. Castillo, Open issues in the linear and nonlinear rheology of wormlike micelles, Curr. Opin. Colloid Interface Sci. 77 (2025) 101919, https:// doi.org/10.1016/i.cocis.2025.101919.
- [44] S.E. Anachkov, G.S. Georgieva, L. Abezgauz, D. Danino, P.A. Kralchevsky, Viscosity peak due to shape transition from wormlike to disklike micelles: effect of dodecanoic acid, Langmuir 34 (2018) 4897–4907, https://doi.org/10.1021/acs. langmuir.8b00421.
- [45] I. Cusano, A. Azarpour, L. Laugeni, S.R. Spena, P.R. Gonzalez, D. Danino, N. Grizzuti, G. Zanchetta, R. Pasquino, Exploring the onset of the nonlinear start-up response of wormlike micelles through rheology and rheo-microscopy: Banding & scission, J. Colloid Interface Sci. 696 (2025) 137725, https://doi.org/10.1016/j. jcis.2025.137725.
- [46] W.P. Cox, E.H. Merz, Correlation of dynamic and steady flow viscosities, J. Polym. Sci. 28 (1958) 619–622, https://doi.org/10.1002/pol.1958.1202811812.
- [47] I. Couillet, T. Hughes, G. Maitland, F. Candau, S.J. Candau, Growth and scission energy of wormlike micelles formed by a cationic surfactant with long unsaturated tails, Langmuir 20 (2004) 9541–9550, https://doi.org/10.1021/la049046m.
- [48] J.D. Peterson, M.E. Cates, Constitutive models for well-entangled living polymers beyond the fast-breaking limit, J. Rheol. 65 (2021) 633–662, https://doi.org/ 10.1122/8.0000199.